AMERICAN SOCIETY FOR MICROBIOLOGY | Applied and Environmental Microbiology

Check for updates

| Environmental Microbiology | Full-Length Text

Mode of carbon and energy metabolism shifts lipid composition in the thermoacidophile *Acidianus*

Jeemin H. Rhim,[1,2] Alice Zhou,[1] Maximiliano J. Amenabar,[3] Grayson M. Boyer,[4] Felix J. Elling,[5,6] Yuki Weber,[5] Ann Pearson,[5] Eric S. Boyd,[3] William D. Leavitt[1,7]

AUTHOR AFFILIATIONS See affiliation list on p. 12.

ABSTRACT The degree of cyclization, or ring index (RI), in archaeal glycerol dibiphytanyl glycerol tetraether (GDGT) lipids was long thought to reflect homeoviscous adaptation to temperature. However, more recent experiments show that other factors (e.g., pH, growth phase, and energy flux) can also affect membrane composition. The main objective of this study was to investigate the effect of carbon and energy metabolism on membrane cyclization. To do so, we cultivated *Acidianus* sp. DS80, a metabolically flexible and thermoacidophilic archaeon, on different electron donor, acceptor, and carbon source combinations ($S^0/Fe^{3+}/CO_2$, $H_2/Fe^{3+}/CO_2$, $H_2/S^0/CO_2$, or H_2/S^0/glucose). We show that differences in energy and carbon metabolism can result in over a full unit of change in RI in the thermoacidophile *Acidianus* sp. DS80. The patterns in RI correlated with the normalized electron transfer rate between the electron donor and acceptor and did not always align with thermodynamic predictions of energy yield. In light of this, we discuss other factors that may affect the kinetics of cellular energy metabolism: electron transfer chain (ETC) efficiency, location of ETC reaction components (cytoplasmic *vs.* extracellular), and the physical state of electron donors and acceptors (gas *vs.* solid). Furthermore, the assimilation of a more reduced form of carbon during heterotrophy appears to decrease the demand for reducing equivalents during lipid biosynthesis, resulting in lower RI. Together, these results point to the fundamental role of the cellular energy state in dictating GDGT cyclization, with those cells experiencing greater energy limitation synthesizing more cyclized GDGTs.

IMPORTANCE Some archaea make unique membrane-spanning lipids with different numbers of five- or six-membered rings in the core structure, which modulate membrane fluidity and permeability. Changes in membrane core lipid composition reflect the fundamental adaptation strategies of archaea in response to stress, but multiple environmental and physiological factors may affect the needs for membrane fluidity and permeability. In this study, we tested how *Acidianus* sp. DS80 changed its core lipid composition when grown with different electron donor/acceptor pairs. We show that changes in energy and carbon metabolisms significantly affected the relative abundance of rings in the core lipids of DS80. These observations highlight the need to better constrain metabolic parameters, in addition to environmental factors, which may influence changes in membrane physiology in Archaea. Such consideration would be particularly important for studying archaeal lipids from habitats that experience frequent environmental fluctuations and/or where metabolically diverse archaea thrive.

KEYWORDS Archaea, DS80, glycerol dibiphytanyl glycerol tetraether, GDGT, ring index, biomarker

The cell membrane is essential for all forms of life, serving as a physical barrier that controls the flow of nutrients and other substances to and from the

Editor John R. Spear, Colorado School of Mines, Golden, Colorado, USA

Address correspondence to Jeemin H. Rhim, jrhim@ucsb.edu.

Jeemin H. Rhim and Alice Zhou contributed equally to this article. Author order was determined on the basis of the amount of contribution to writing.

The authors declare no conflict of interest.

See the funding table on p. 12.

Received 9 August 2023
Accepted 1 December 2023
Published 18 January 2024

external environment. Membranes also have an important bioenergetic function, as the electrochemical gradient across the cell membrane can be harnessed to conserve energy (ATP synthesis) or to perform work. Hence, the ability to modify membrane fluidity and permeability (homeoviscous adaptation) in response to changing environments is crucial for cell survival and growth. Cells can achieve this by modifying their lipid membrane composition (1). While homeoviscous adaptation strategies are found across all three domains of life, Archaea provide a unique perspective to our understanding of this process. This is because archaeal lipids are fundamentally different from those of Bacteria and Eukarya, and many Archaea thrive in extreme habitats that commonly experience environmental fluctuations.

Many Archaea synthesize membrane-spanning lipids known as glycerol dibiphytanyl glycerol tetraethers (GDGTs; Fig. 1). These unique structures are abundant in the core lipids produced by many thermophilic archaea (2) and comprise nearly all of the lipid membranes of acidophilic archaea (3, 4). GDGTs form very stable monolayers characterized by high packing efficiencies, high transition temperatures, and low permeabilities (5–8). Incorporation of cyclopentane or cyclohexane rings in the alkyl cores of GDGTs further increases membrane packing and transition temperatures and helps maintain membrane integrity under extreme conditions (5, 7).

Besides having key physiological functions, archaeal GDGTs can serve as biomarkers that have useful applications in Earth sciences and astrobiology. Due to their high preservation potential in sediments (up to millions of years) and the information that can be inferred from the degree of cyclization, archaeal GDGTs have been widely applied as paleoenvironmental proxies [e.g., references (9–12)]. Many Archaea often belong to deeply rooted phylogenetic lineages (13–15) and thus also provide contemporary analogs to study the processes that supported early life forms on Earth. Furthermore, Archaea that are well adapted to extreme environments can serve as model systems for astrobiology, as they allow us to explore the range of physicochemical conditions habitable to life (16).

Controlled laboratory experiments are crucial for advancing the understanding of homeoviscous adaptation in Archaea and improving the ability to interpret GDGT biomarkers. Studies to date have investigated a variety of factors affecting the degree of cyclization in archaeal lipids. Some of these factors include temperature (17–24), pH (3,

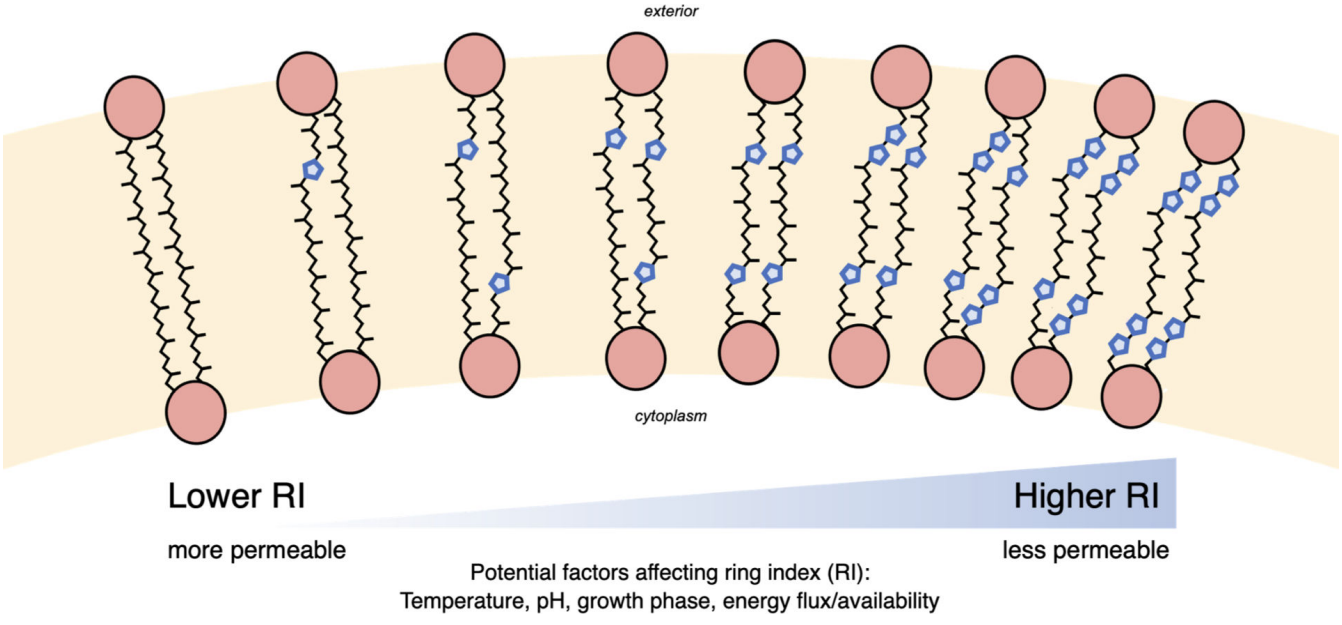

FIG 1 The core GDGT lipid structures may contain between 0 and 8 pentacyclic rings. An increase in the average number of rings per GDGT, or an increased RI, is generally associated with increased membrane packing and decreased permeability.

18, 22–24), ionic strength or salinity (18, 22), oxygen availability (24, 25), growth rate or energy flux (26–28), and growth phase (23, 29, 30). In general, higher degrees of GDGT cyclization are associated with higher temperature, lower pH, and factors that reflect or lead to increased physiological or energetic stress (Fig. 1). For example, several strains of marine ammonia-oxidizing archaea *Nitrosopumilus maritimus* and a thermoacidophile *Sulfolobus acidocaldarius* produced GDGTs with higher RIs with decreasing O_2 availability (24, 25). RIs are also observed to increase at late growth phases in both thermoacidophilic and mesophilic archaea (23, 29), hinting that increasing membrane packing might be a common response among Archaea to nutrient and/or energy limitation. Moreover, continuous culture experiments showed that RIs increase significantly as growth or metabolic rate and energy flux decrease (26–28).

The interplay among the factors affecting membrane cyclization is particularly important for polyextremophiles that are adapted to multiple extremes, as different environmental and physiological factors could require different extents of lipid cyclization. The effects of individual parameters, such as temperature, pH, ionic strength, and oxygen flux on the lipids of thermoacidophilic archaea, have been investigated in previous studies [e.g., references (18, 24)]. While these studies inform us about how RIs reflect various physicochemical factors, the effects of energy and carbon metabolism on membrane composition are poorly understood. This is partly because testing such factors requires an organism that has a flexible energy and carbon metabolism. In this study, we focus on a metabolically flexible and thermoacidophilic archaeon *Acidianus* sp. DS80 (hereafter DS80) that can use several combinations of soluble and insoluble electron donors and acceptors to support both chemolithoautotrophic and chemoheterotrophic growth (31–33). DS80 was isolated from a geochemically dynamic (34) and acidic hot spring, "Dragon Spring," in Yellowstone National Park, Wyoming, USA (31). The strain grows optimally at 80 °C and pH 3.0 (31). When grown autotrophically, DS80 can use molecular hydrogen (H_2) or elemental sulfur (S^0) as an electron donor coupled to S^0 or ferric iron (Fe^{3+}) as an electron acceptor. In addition to its ability to grow as a chemoautotroph, DS80 can also grow as an aerobic or anaerobic heterotroph. In the case of anaerobic heterotrophy, H_2 is additionally required when S^0 is provided as the electron acceptor (i.e., chemolithoheterotrophy; inorganic energy source with organic carbon source) (32, 33). The metabolic plasticity of DS80 provides a unique opportunity to investigate how different energy and carbon metabolisms in a thermoacidophilic archaeon affect lipid membrane composition.

The metabolic versatility of DS80 also raises the intriguing question as to how it selects among the multiple available substrates in its natural habitat to support its metabolism. Amenabar et al. (31) characterized the thermodynamics and kinetics of substrate transformation by DS80 to explore the relationship between bioenergetics and carbon fixation efficiency (31). They made a counterintuitive observation where the least energetically favorable redox couple (H_2/S^0), or that which provided the least energy per electron transfer, resulted in the greatest degree of carbon assimilation and biomass synthesis per unit energy expended (31). Both of these bioenergetic parameters are likely relevant for membrane adaptations and cyclization, independent of or in concert with the established environmental drivers such as temperature and pH.

We predict that the energy available to DS80 from different electron donor/acceptor pairs and the energy demand required to access different types of electron donors and acceptors both affect core lipid composition and cyclization. To test this hypothesis, we cultivated DS80 with different electron donors and electron acceptors, both autotrophically and heterotrophically, while holding the pH of the growth medium and the incubation temperature constant. Below we document these findings with respect to studies on DS80's energy metabolism and in light of other findings as to the role of energy availability on archaeal membrane adaptation.

RESULTS

Acidianus sp. strain DS80 was cultured as a chemolithoautotroph on three different electron donor/acceptor pairs (H_2/S^0, H_2/Fe^{3+}, and S^0/Fe^{3+}) with CO_2 as the carbon source, and as a chemolithoheterotroph on H_2/S^0 with glucose as the carbon source (Table 1). Figure 2A shows that the rate of Fe^{2+} production decreases as the total [Fe^{2+}] approaches the starting [Fe^{3+}]. This suggests that Fe^{3+} was the limiting factor under Fe^{3+}-reducing conditions ($H_2/Fe^{3+}/CO_2$ and $S^0/Fe^{3+}/CO_2$), as expected from the available electron donor and acceptor concentrations and reaction stoichiometries (equations 3 and 4). On the other hand, we did not observe quantitative consumption of H_2 under S^0-reducing conditions ($H_2/S^0/CO_2$ and H_2/S^0/glucose). For example, for the $H_2/S^0/CO_2$ treatment, S^{2-} production decreases as the total [S^{2-}] approaches 6 mM (Fig. 2A); ca. 98 millimoles of H_2 was initially provided in the headspace, which could produce up to ca. 49 mM [S^{2-}] upon quantitative consumption of H_2. Thus, a factor other than electron donor/acceptor availability likely limits growth under this condition. One such factor is the production of H_2S, which has been shown to be toxic at far lower (<80 µM) concentrations in the thermoacidophilic S^0-reducing archaeon *Thermoproteus* strain CP80 (35). It is possible that high concentrations of the uncharged molecule can diffuse across the membrane (36) only to deprotonate in the more circumneutral cytoplasm (the pK_a of H_2S/HS^- is 6.4 at 80 °C) (37). This would result in acidification of the cytoplasm much like has been observed with organic acids [e.g., reference (38)].

The lipid compositions of DS80 vary across different growth conditions. The degree of cyclization (i.e., RI) changed consistently with metabolite production rates and electron transfer rates (Table 2; Fig. 3). Overall, the core lipid profiles of DS80 primarily consisted of GDGT-4 and GDGT-5. The Fe^{3+}-reducing conditions ($H_2/Fe^{3+}/CO_2$ and $S^0/Fe^{3+}/CO_2$) resulted in higher relative abundances of GDGT-4, GDGT-5, and GDGT-6 than the S^0-reducing conditions (Fig. 3). Consequently, Fe^{3+}-reducing conditions resulted in higher RI values compared to S^0-reducing conditions (H_2/S^0/glucose and $H_2/S^0/CO_2$). There was more than a full unit difference between the highest (4.71 ± 0.01) and lowest (3.61 ± 0.08) RIs observed in cultures grown on $S^0/Fe^{3+}/CO_2$ and H_2/S^0/glucose,

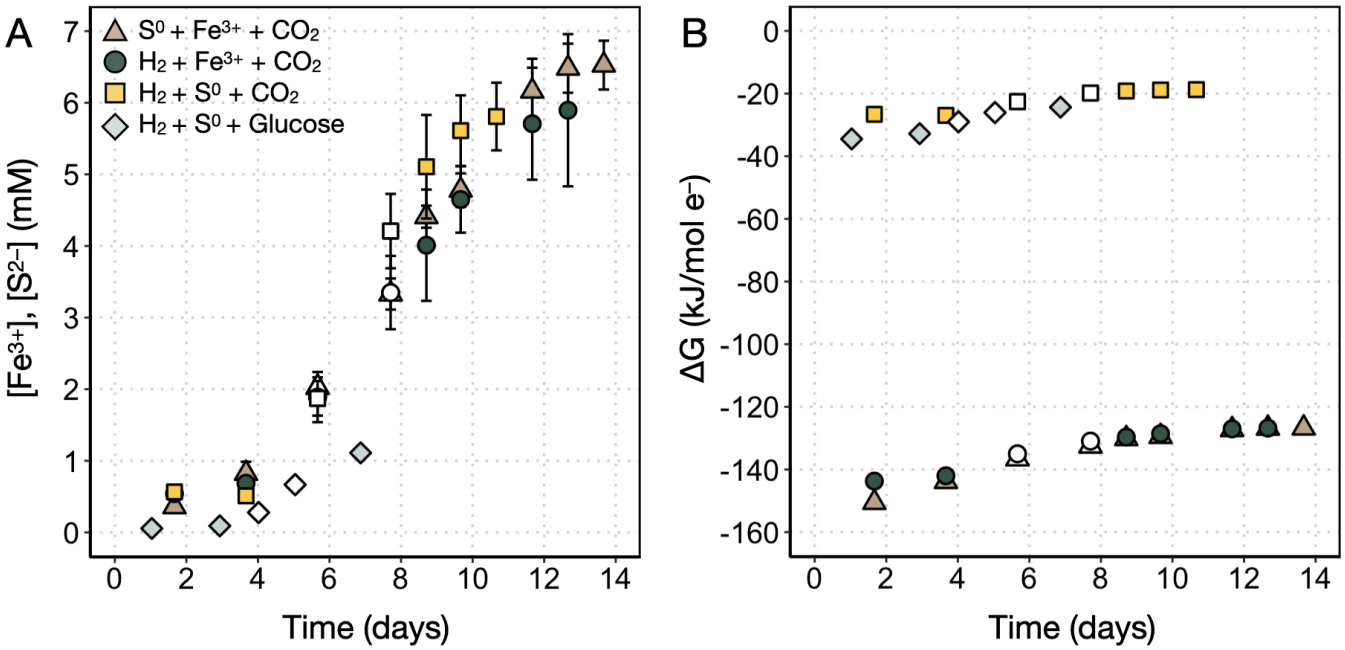

FIG 2 Production of metabolites and available (calculated) Gibbs free energy during growth of *Acidianus* sp. strain DS80. (A) Changes in the concentration of metabolites (Fe^{2+} or S^{2-}) as a function of incubation time. Error bars reflect the standard deviation of measurements from three biological replicates. (B) Available Gibbs free energy (Δ*G*) per mole of electrons transferred based on calculations and equations 2–4. Open symbols represent logarithmic metabolite production (and by proxy, growth) and are the data points used to calculate ΔG_{Log} values and metabolite production rates in Table 2.

TABLE 1 Redox couples from which GDGTs were retrieved in this study

Experimental condition	Electron donor	Electron acceptor	Carbon source
$S^0/Fe^{3+}/CO_2$	S^0 (s) (5 g/L)	Fe^{3+} (7 mM)	CO_2 (g) (20%, vol/vol)
$H_2/Fe^{3+}/CO_2$	H_2 (g) (80%, vol/vol)	Fe^{3+} (7 mM)	CO_2 (g) (20%, vol/vol)
$H_2/S^0/CO_2$	H_2 (g) (80%, vol/vol)	S^0 (s) (5 g/L)	CO_2 (g) (20%, vol/vol)
H_2/S^0/glucose	H_2 (g) (80%, vol/vol)	S^0 (s) (5 g/L)	Glucose (s) (5 mM)

respectively (Table 2; Fig. 3). Between the two S^0-reducing conditions, the heterotrophic condition resulted in a significantly lower RI (3.61 ± 0.08; H_2/S^0/glucose) compared to the autotrophic condition (3.89 ± 0.14; $H_2/S^0/CO_2$), although the calculated available Gibbs free energy during log phase (termed ΔG_{Log} herein) for the two conditions were comparable. Overall, the trends observed in RIs were better explained by the normalized electron transfer rate ($R^2 = 0.94$; Fig. 4B) than by the ΔG_{Log} values ($R^2 = 0.59$; Fig. 4A).

DISCUSSION

For (poly)extremophilic archaea (39), the balance between bioenergetics and membrane plasticity becomes particularly important for survival and growth. On one hand, ring synthesis reduces the demand for electrons (and thus electron donors/acceptors), as the reduction of double bonds during saturation (opposite of cyclization) requires a net expenditure of reducing equivalents (26, 40). As such, under electron donor or acceptor (energy or electron) limitation, a higher degree of cyclization helps to minimize the expenditure of reducing equivalents during lipid synthesis and provides tighter membrane packing that reduces leakage of ions across the cell membrane (41). On the other hand, factors such as the nature of electron donors or acceptors (e.g., soluble *vs.* insoluble or charged *vs.* uncharged) may impose an opposing biosynthetic pressure to maintain a lower degree of cyclization. A recent study reported changes in bacterial lipid composition as a function of electron acceptor (nitrate *vs.* manganese dioxide), and the changes were attributed to the differences in the electron transport chains (ETC) embedded in the cell membrane (42). For archaeal lipids, changes in the membrane composition in response to the extent of anaerobiosis (e.g., S^0 *vs.* O_2 as the electron acceptor) have been observed (43). While homeoviscous adaptations in Archaea have been studied in the context of different environmental and physiological forcings (17–23, 25–29), it remains poorly understood how cells accommodate bioenergetic needs while balancing needs for different electron donors/acceptors and how this is reflected in cyclization patterns in GDGT lipids.

In this study, the metabolic versatility of DS80 allowed us to begin to investigate archaeal membrane GDGT cyclization patterns during growth on various electron donor/acceptor pairs while keeping temperature, pH, and growth phase at the time of biomass

TABLE 2 Summary of bioenergetics, metabolite production rates, and ring indices across all conditions tested in this study

Condition	ΔG_{Log}[a] (kJ/mol e^-)	Avg. metabolite production rate (mmol/L/day)[b]	Avg. electron transfer rate (mmol e^-/L/day)[c]	Inferred cell-specific metabolite production rate (fmol/cell/day)[d]	Ring index[e]
$S^0/Fe^{3+}/CO_2$	−135	0.39 ± 0.05	2.37 ± 0.28	62 ± 10	4.71 ± 0.03
$H_2/Fe^{3+}/CO_2$	−133	0.38 ± 0.08	0.77 ± 0.16	52 ± 9	4.10 ± 0.09
$H_2/S^0/CO_2$	−21	0.44 ± 0.16	0.87 ± 0.32	7 ± 1	3.89 ± 0.14
H_2/S^0/glucose	−28	0.10 ± 0.04	0.20 ± 0.09	n/a	3.61 ± 0.11

[a]Average Δ*G* values for data points representing logarithmic increase in metabolite concentration (open symbols in Fig. 2). For the H_2/S^0/glucose condition, it is assumed that glucose does not significantly contribute to energetic Δ*G*. See Bioenergetic calculations for a detailed description of values used for Δ*G* calculations. See Table S2 for individual sample data.
[b]Rates of Fe^{2+} production per liter for the $S^0/Fe^{3+}/CO_2$ and $H_2/Fe^{3+}/CO_2$ conditions, based on the Ferrozine assay results; rate of S^{2-} production per liter for the $H_2/S^0/CO_2$ condition, based on the methylene blue assay results (dissolved concentration) and applying a standard gas-phase equilibrium correction to calculate total sulfide.
[c]Rates of electrons transferred per liter of culture, based on metabolite production rates and reaction stoichiometries in equations 2–4.
[d]Metabolite production rates were divided by inferred cell density values. Cell density values were calculated from measured metabolite concentrations, [Fe^{2+}] or [S^{2-}], and the growth yield calculated for logarithmic growth from the data reported in reference (31): 2.5×10^{12} cells per mole of Fe^{2+} produced for $S^0/Fe^{3+}/CO_2$; 3.0×10^{12} cells per mole of Fe^{2+} produced for $H_2/Fe^{3+}/CO_2$; 20.6×10^{12} cells per mole of S^{2-} produced for $H_2/S^0/CO_2$. n/a = not available.
[e]Ring indices were calculated from biomass harvested during late logarithmic or early stationary phase.

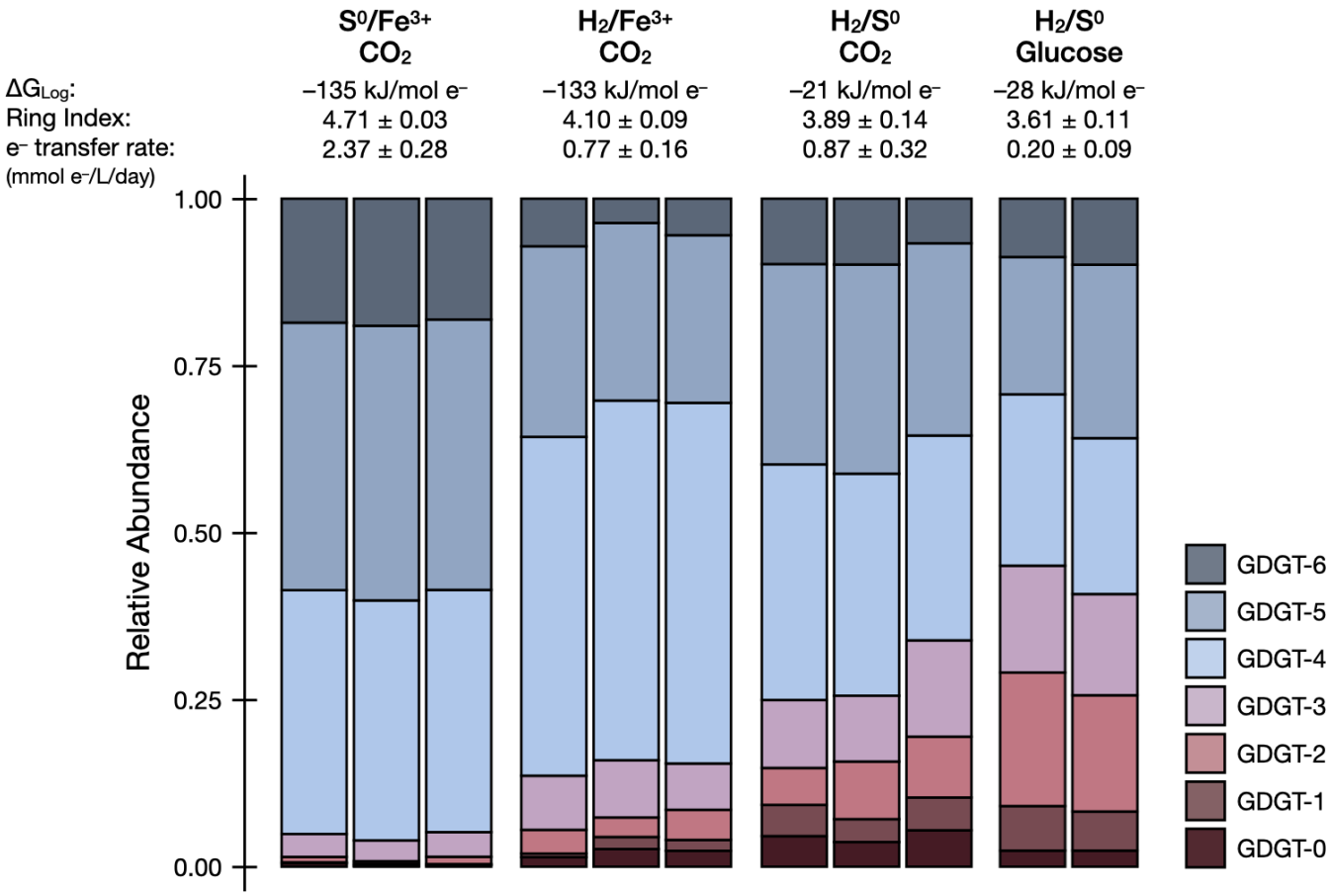

FIG 3 Relative abundances of core GDGT lipids as a function of electron donor/electron acceptor couples and carbon sources provided. The available Gibbs free energy during the log phase (ΔG_{Log}), average ring index (the weighted average degree of cyclization), and normalized electron transfer rates for each condition are shown above the corresponding stacked bar charts.

collection consistent across treatments. When the thermodynamic predictions of energy yield from the tested redox couples are combined with the bioenergetics argument to increase membrane packing (i.e., increased RI) under energy limitation, we expect the highest RI to be measured in culture conditions with the least favorable ΔG_{Log} values ($H_2/S^0/CO_2$ and H_2/S^0/glucose). Counterintuitively, we observed that the $H_2/S^0/CO_2$ and H_2/S^0/glucose treatments yielded the lowest RIs averaging 3.89 ± 0.14 and 3.61 ± 0.08, respectively (Table 2; Fig. 3). Interestingly, the treatment with more favorable ΔG_{Log} values ($H_2/Fe^{3+}/CO_2$ and $S^0/Fe^{3+}/CO_2$) yielded higher RIs averaging 4.10 ± 0.09 and 4.71 ± 0.03, respectively (Table 2; Fig. 3). The difference of over a full unit of RI observed in this study is comparable to the magnitude of changes observed upon significant shifts in temperature (15°C–20°C shift) or pH (e.g., nearly 2 log shift) (18, 44).

We propose that the trends in membrane cyclization patterns in DS80 reflect differences in energy demand associated with the nature and availability of electron donors and acceptors that are not accounted for in thermodynamic calculations. In general, we observed comparatively lower RIs during S^0 reduction compared to those during Fe^{3+} reduction. In the case of carbon assimilation and biomass production, Amenabar et al. (31) identified the difference in electron transfer efficiency as the primary factor underlying the counterintuitive observation of the highest biomass yield during S^0 reduction (31). For the H_2/S^0 redox couple, electrons are transferred via an extremely short ETC involving a membrane-bound [NiFe]-hydrogenase and sulfur reductase (SRE) complex linked by a quinone cycle (45). Interestingly, electron transfer efficiency was significantly correlated with membrane cyclization in DS80 as determined

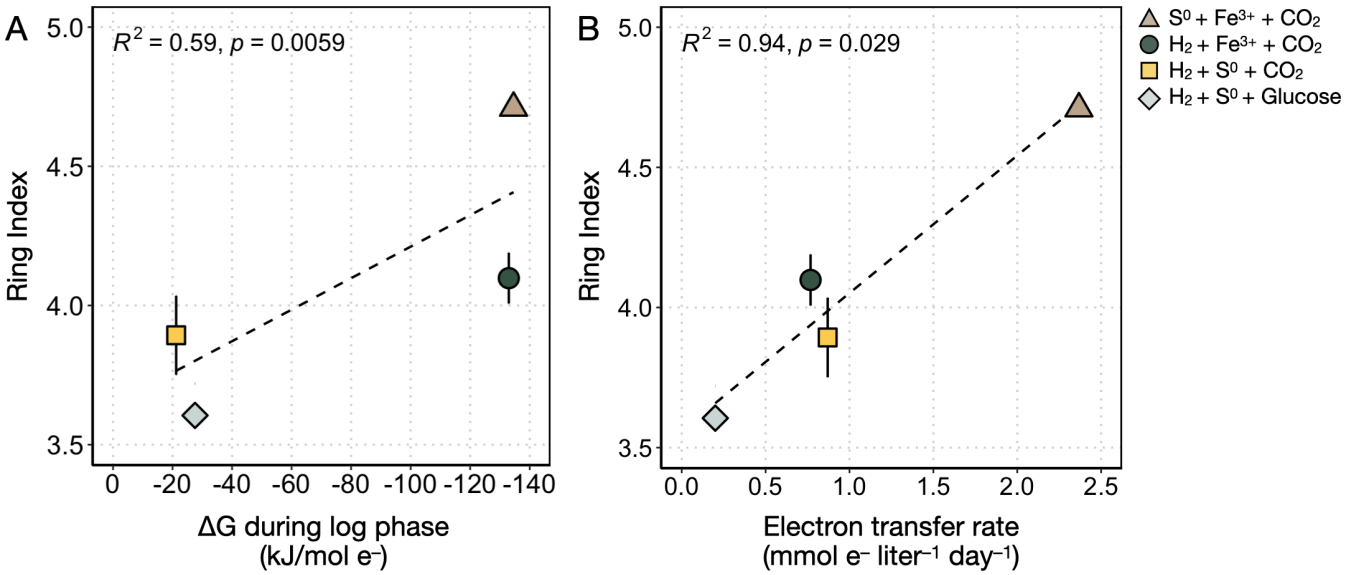

FIG 4 Average ring index values as a function of available Gibbs free energy and electron transfer rate. (A) The Δ*G* values reflect calculations made during logarithmic growth (ΔG_{Log}) for each condition tested in this study (see Bioenergetic calculations). (B) Electron transfer rates were calculated from the measured rates of Fe^{2+} or S^{2-} production per liter of culture during logarithmic growth and using reaction stoichiometries in equations 2–4. The R^2 and *p* values in each panel are for the regression line (dashed lines) for all average ring index values.

herein, where lower electron transfer efficiency during Fe^{3+} reduction is compensated by higher cyclization to presumably decrease the expenditure of reducing equivalents when compared to growth on S^0. This suggests that the nature of electron donors and acceptors and microbial adaptations to extract or donate electrons to those substrates both affect lipid composition.

The treatments with the lowest and highest RIs (H_2/S^0/glucose and S^0/Fe^{3+}/CO_2, respectively; Table 2; Fig. 3) can be further examined in the context of the location of where the redox reactions (electron transfers) are taking place. The membrane-bound SRE complex that facilitates sulfur reduction in a closely related strain *Acidianus ambivalens* (and likely DS80) is extracellularly oriented, meaning that reduction takes place outside of the cell (32, 45, 46). In contrast, the unique sulfur oxygenase reductase (SOR) complex facilitates cytoplasmic oxidation of sulfur in a few lineages of *Sulfolobales* including *Acidianus* (46–48). The protein responsible for S^0 transport into the cell remains unidentified, and the source of intracellular sulfur for the SOR system is not well understood. It has been suggested that the sulfide:quinone oxidoreductase (SQO) may serve as the intracellular sulfur source by forming polysulfide chains from the oxidation of hydrogen sulfide (46). Whether it is via an unknown transporter for S^0 and/or via polysulfide formation by SQO, cytoplasmic sulfur oxidation via the SOR system would require additional energy expenditure (i.e., higher RI is favorable) to account for sulfur acquisition. Furthermore, the number of enzymes/proteins involved in the oxidation of sulfur via SOR to generate energy (24 subunits) (48) *vs.* the reduction of sulfur via SRE (five subunits) (45) would impose an additional biosynthetic burden on cells oxidizing S^0. Besides the SOR complex, many other enzymes are required during the oxidative metabolism of S^0, which would further increase the energy demands associated with extracting electrons from this substrate. Overall, the energy expenditures expected for intracellular sulfur oxidation and extracellular sulfur reduction align with the highest and lowest RIs observed from the S^0/Fe^{3+}/CO_2 and H_2/S^0/glucose conditions, respectively.

In addition to the additional energy expenditures associated with S^0 oxidation, lower energy efficiency during Fe^{3+} reduction may also contribute to the high RI observed in the S^0/Fe^{3+}/CO_2 treatment. Previous work has shown that DS80 can reduce soluble Fe^{3+} produced by acidic dissolution of ferric iron minerals (33) or directly reduce Fe^{3+} on

the mineral surface (49) during dissimilatory iron reduction (DIR). Electron transfer likely takes place outside of the cell during DIR given that DS80 produces pili-like structures exclusively during DIR and that it lacks biochemically characterized or bioinformatically identified genes encoding for *c*-type cytochromes (31). Moreover, intracellular production of Fe^{2+} during DIR would likely be toxic to cells (50). While the exact location and mechanism of the electron transfer to Fe^{3+} in DS80 remain unknown, extracellular electron transfer during DIR may be possible through a non-dedicated mechanism where electrons diverted from the membrane spontaneously reduce Fe^{3+}. A similar mechanism has been shown in methanogens during pyrite (FeS_2) reduction, where membrane electrons with low (<280 mV) redox potentials are diverted toward the reduction of FeS_2 (51). Regardless of the exact mechanism, these plausible routes of extracellular electron transfer during DIR are inefficient and further contribute to energy limitation, and subsequently, the highest RI in this study.

Besides the impact of electron donors/acceptors and associated electron transfer pathways, carbon metabolism also appears to contribute to changes in membrane cyclization. It has been shown that when S^0 is provided to DS80 as the electron acceptor, inorganic and organic carbon sources could only support growth when H_2 was also provided (32). Considering the obligate requirement for H_2 during chemolithoheterotrophic metabolism during S^0 reduction and the insignificant difference in the yield of cells when grown with $H_2/CO_2/S^0$ compared to $H_2/CO_2/S^0$ supplemented with acetate (32), we assumed no significant energetic ΔG contribution from glucose for the H_2/S^0/glucose treatment. Accordingly, the ΔG_{Log} values estimated for the $H_2/S^0/CO_2$ and H_2/S^0/glucose conditions are comparable (Fig. 2B; Table 2), and thus the RIs would be expected to be comparable if they were only influenced by this parameter. However, it is possible that some or all of the carbon used for lipid biosynthesis originates from glucose during chemolithoheterotrophic growth. When lipid synthesis starts from a more reduced form of carbon, the demand for reducing equivalents during lipid synthesis would be lower. This is in line with the difference in RIs observed between the autotrophic $H_2/S^0/CO_2$ (3.89 ± 0.14) and heterotrophic H_2/S^0/glucose (3.61 ± 0.08) conditions (Table 2; Fig. 3).

Overall, the additional considerations above provide a better explanation for the cyclization patterns observed in this study (Fig. 3). These collective considerations are also consistent with the observation that RIs correlate better with electron transfer rates ($R^2 = 0.94$) than with calculated ΔG_{Log} values ($R^2 = 0.59$) (Fig. 4), as metabolic rates reflect a net physiological response to environmental forcings. While cell abundance was not quantified in this study, the growth yield for each autotrophic condition can be inferred from the data reported by Amenabar et al. (31). Assuming the same growth yield for the autotrophic and heterotrophic H_2/S^0 treatments ($H_2/S^0/CO_2$ and H_2/S^0/glucose), the correlation is still significant ($R^2 = 0.94$) between RIs and cell-specific electron transfer rates (i.e., metabolic rates normalized to both reaction stoichiometry and biomass yield) (Fig. S2).

The lower RIs at lower electron transfer rates observed in this study (Fig. 4B) appear to contradict observations from previous studies where higher RIs were observed at lower metabolic rates or stationary growth phase. However, upon closer consideration, the combined observations reveal a broader link between energy limitation and membrane cyclization. In experiments with the thermoacidophile *S. acidocaldarius*, both in fed-batch cultures with electron acceptor limitation and continuous cultures with electron donor limitation, slower cellular doubling times and higher RIs were observed (24, 27, 28). Similarly, in continuous cultures of *N. maritimus*, electron donor limitation resulted in slower growth and cell-specific ammonia oxidation rates as well as higher RIs (26). Both *S. acidocaldarius* and *N. maritimus* continuous culture experiment results are consistent with previous batch culture experiments where, when energy limitation is expected during the lag or stationary growth phase, higher RIs were observed (23, 29, 30). The general trends from prior batch and continuous culture studies are directly in line with the bioenergetics prediction of increased membrane packing (higher RI) under energy limitation, often co-occurring with a slower metabolic rate or lag/stationary

growth phase. Unlike other batch experiments, biomass was harvested at about the same growth phase across experiments in this study. Furthermore, DS80 was grown on a range of different electron donor/acceptor pairs to test the effect of energy and carbon metabolism on membrane cyclization, whereas the batch and continuous culture studies noted above tested the effect of metabolic rate or growth phase within the same metabolic regime. The trend we observe reflects the differential energy limitation experienced by DS80 in the broader context of differences—in ETC efficiency, location of redox chemistry, and physical state of substrate—across energy and carbon metabolism modes. Together, the work here with DS80 and prior studies across GDGT-producing archaea highlight the role that carbon and energy metabolism (electron transfer efficiency, in particular) play in shaping GDGT cyclization and archaeal membrane physiology in nature.

In this study, we used a metabolically flexible thermoacidophilic archaeon *Acidianus* sp. DS80 to test the effects of energy and carbon metabolism on membrane cyclization. Experimental results revealed that both the metabolite production rate and the degree of cyclization varied across growth treatments. However, the patterns in RI did not always correlate with the ΔG_{Log} values for corresponding redox couples. We discussed several factors that may affect reaction kinetics during the growth of DS80 and that may influence RI. The generally lower RI observed in S^0-reducing conditions can be attributed to the (i) high efficiency of the short electron transfer pathway involving a [NiFe]-hydrogenase and sulfur reductase linked by quinone, (ii) favorable location of redox chemistry during S^0 reduction, and (iii) potential need to maintain membrane fluidity for substrate diffusion during H_2 oxidation. Moreover, carbon metabolism appears to affect membrane cyclization, where assimilation of a more reduced form of carbon (glucose vs CO_2) during heterotrophy results in lower RI compared to autotrophic conditions. Altogether, these findings highlight the effects of energy and carbon metabolism on membrane cyclization in DS80 in the same or opposite direction of the biosynthetic pressure imposed by extreme temperature and pH. Taken together, factors that increase the energetic demands on cells (less efficient ETCs, autotrophic metabolism, unfavorable locations of proteins involved in redox chemistry) appear to generally result in increased cyclization of GDGT lipids (i.e., GDGT RI). Further understanding the complex interplay among environmental and physiological factors that influence patterns of GDGT cyclization will improve the application of archaeal GDGTs as records of past environments.

MATERIALS AND METHODS

Strain and cultivation procedures

To examine the effect of carbon sources, electron donors, and electron acceptors on the composition of GDGT lipids, axenic cultures of DS80 were grown on a defined mineral medium (52) consisting of NH_4Cl (0.33 g/L), KCl (0.33 g/L), $CaCl_2 \cdot 2H_2O$ (0.33 g/L), $MgCl_2 \cdot 6H_2O$ (0.33 g/L), and KH_2PO_4 (0.33 g/L). Following autoclave sterilization, filter-sterilized Wolfe's vitamins (1 mL/L) and SL-10 trace metals (1 mL/L) were added to the base mineral medium. Electron donors and electron acceptors were then added after autoclave sterilization, according to each experimental condition (Table 1). Elemental sulfur (S^0; sulfur precipitated powder, EMD Millipore) was sterilized by baking at 100°C for 24 hours and added to the medium at a concentration of 5.0 g/L. Ferric iron (Fe^{3+}) was added in the form of ferric sulfate solution to a final concentration of 7 mM. Importantly, DS80 is unable to respire sulfate but can respire ferric iron; sulfate from ferric sulfate or sulfide (from S^0 reduction) can serve as sulfur sources for DS80 (31).

The overall medium preparation for autotrophic cultures (H_2/S^0, H_2/Fe^{3+}, and S^0/Fe^{3+}) followed a previously described protocol involving 2 hours of purging with sterile N_2 gas followed by replacement of the headspace with sterile H_2/CO_2 (80:20, vol/vol) or N_2/CO_2 (80:20, vol/vol) (31, 32). Three biological replicates were prepared for each experimental condition in 5 L glass bottles (Fisherbrand, FB-800-5000), each with a final liquid volume

of 2 L and sealed with butyl rubber stoppers. Each bottle was inoculated with 200 mL of a log phase culture of DS80 and incubated statically at 80 °C (Binder Avantgarde BD56). The pH of the growth medium was set at an initial value of 3.0 for all conditions and remained within 0.1 units throughout the experiment (data not shown). Medium preparation for heterotrophic cultures (H_2/S^0/glucose) followed the general procedure described above and was distributed into smaller individual 160 mL serum bottles, each with a final liquid volume of 100 mL. Each serum bottle was additionally amended with a sterile glucose solution to a final concentration of 5 mM.

Based on the stoichiometry shown in equation 2a, 5 g/L of S^0 would meet the theoretical requirement for complete oxidation of the H_2 supplemented in S^0-reducing conditions (H_2/S^0/CO_2 and H_2/S^0/glucose). Based on the stoichiometry shown in equations 3 and 4, 5 g per L of S^0 and 80% H_2 in the 2.88 L headspace would meet the theoretical requirement for complete reduction of the Fe^{3+} supplemented in Fe^{3+}-reducing conditions (S^0/Fe^{3+}/CO_2 and H_2/Fe^{3+}/CO_2).

Measurement of metabolic activities

The growth of microbial cultures is traditionally assessed using direct cell counts or optical density measurements. In this study, the production of total sulfide or ferrous iron was used as a proxy for microbial growth since they have previously been shown to correlate strongly and positively with cell densities (31, 32). Concentrations of dissolved sulfide were determined via the methylene blue reduction method (53) for H_2/S^0 cultures. The amount of total sulfide produced was calculated from the dissolved concentrations using standard gas-phase equilibrium (equation 2b) calculation (52). Concentrations of reduced iron (Fe^{2+}) were determined via the ferrozine assay (54) for cells provided with H_2/Fe^{3+} or S^0/Fe^{3+} (Fig. S1). Metabolic rates were calculated based on the results of the aforementioned assays (Fig. S1).

Lipid analyses

All DS80 biomass samples were harvested via filtration upon reaching the late logarithmic or early stationary phase, based on measurements of metabolites and comparisons to previous growth curves (31, 32). Cultures were removed from the incubator and rapidly cooled to room temperature in 4 °C water baths. Cooled samples were then filtered onto 0.22 µm pore size glass fiber filters (Advantec GF7547MM Grade GF75 Glass Fiber Filters; 47 mm diameter). Prior to use, all glass components were combusted at 350°C for 4 hours. To remove the bulk of solid sulfur and/or iron (oxy)hydroxide precipitates, cultures were decanted into 250 mL centrifuge bottles and spun down gently (3 min at 600 *g*). The resulting supernatant containing suspended cells was concentrated onto glass fiber filters and frozen at –80°C until lipid extractions.

Prior to extraction, filters were cut into small pieces using pre-combusted stainless-steel scissors. One hundred nanograms of synthetic C_{46} GDGT standard (55) was added to each sample for quantification. Samples were hydrolyzed in 5% (vol/vol) methanolic HCl (70 °C, 90 min) to convert intact polar lipids to core lipids. Following acid hydrolysis, core lipids were extracted by ultrasonication after the addition of either dichloromethane (DCM, used for H_2/S^0, H_2/Fe^{3+}, and S^0/Fe^{3+} samples) or methyl tert-butyl ether (used for H_2/S^0/glucose samples). Phase separation was induced with either a 1:1 mixture of DCM and water (H_2/S^0, H_2/Fe^{3+}, and S^0/Fe^{3+} samples) or with hexane (H_2/S^0/glucose samples). Core GDGTs were then purified over activated aluminum oxide by elution with DCM/methanol (1:1, vol/vol). The resulting fraction was dried under a flow of N_2, resuspended in 500 µL hexane/isopropanol (99:1, vol/vol), passed through a 0.45-µm PTFE filter, and stored at –20 °C until analysis.

The extracted core GDGTs were analyzed by ultra high performance liquid chromatography-atmospheric pressure chemical ionization-mass spectrometry (UHPLC-APCI-MS) using an Agilent 1290 Infinity series UHPLC system coupled to an Agilent 6410 triple-quadrupole MS, operated in positive mode (gas temperature: 350 °C; vaporizer temperature: 300 °C; gas flow: 6 L min^{-1}; and nebulizer pressure: 60 psi). Core lipids

in the filtered extract were separated using normal phase liquid chromatography-mass spectrometry. Analytical separation of GDGTs was achieved by injecting 10 µL of total lipid extract onto a Prevail Cyano column maintained at 50 °C. GDGTs were eluted using a linear gradient from 0.2% to 10% (vol/vol) isopropyl alcohol (IPA) in hexane at a flow rate of 0.5 mL/min as previously described (56). At the end of each sample run, the columns were back-flushed with a 70:30 mixture of hexane:IPA (90:10, vol/vol) and IPA:methanol (70:30, vol/vol). Columns were re-equilibrated to initial conditions before proceeding with the next sample run. The MS was operated in single ion monitoring mode (dwell time: 25 ms and fragmentor voltage: 75 V), and GDGTs were quantified by integration of the ion chromatograms of analytes relative to the C_{46} internal standard peak. Peak areas of all GDGT species are provided in Table S1.

Ring index was calculated for each sample according to the formula, following reference (57). The definition below accounts for GDGTs with up to six rings (GDGT-0–GDGT-6), as GDGT-7 and GDGT-8 were not detected

$$\mathrm{RI} = \frac{1\times[\mathrm{GDGT}-1] + 2\times[\mathrm{GDGT}-2] + 3\times[\mathrm{GDGT}-3] + 4\times[\mathrm{GDGT}-4] + 5\times[\mathrm{GDGT}-5] + 6\times[\mathrm{GDGT}-6]}{[\mathrm{GDGT}-0]+[\mathrm{GDGT}-1]+[\mathrm{GDGT}-2]+[\mathrm{GDGT}-3]+[\mathrm{GDGT}-4]+[\mathrm{GDGT}-5]+[\mathrm{GDGT}-6]}. \quad (1)$$

Note that these results do not consider the relative contribution of calditol-linked GDGTs. Zeng et al. (58) observed that calditol-linked lipids are slightly more cyclized compared to GDGTs in *S. acidocaldarius* (58). The acid hydrolysis method used in this study does not remove the ether-bound calditol head group, thus the RIs reported in this study may be underestimated. Based on previous observations [e.g., references (24, 28, 58)], we assume that the relative offset in RIs between experimental conditions, especially among autotrophic conditions, likely will remain consistent between the calditol-linked GDGT pool and the remaining GDGT pool (24).

Bioenergetic calculations

Each experimental growth condition was dependent on one of the following chemical reactions in the medium at pH 3.0:

$$\mathrm{H_2\,(aq)} + \mathrm{S^0\,(s)} \longrightarrow \mathrm{H_2S\,(aq)} \quad (2a)$$

$$\mathrm{H_2S\,(aq)} \leftrightarrow \mathrm{H_2S\,(g)} \quad (2b)$$

$$\mathrm{S^0\,(s) + 6\,Fe^{3+}\,(aq) + 4\,H_2O\,(1)} \longrightarrow \mathrm{6\,Fe^{2+}\,(aq) + HSO_4^-\,(aq) + 7\,H^+} \quad (3)$$

$$\mathrm{H_2\,(aq) + 2\,Fe^{3+}\,(aq)} \longrightarrow \mathrm{2\,Fe^{2+}\,(aq) + 2\,H^+} \quad (4)$$

The amount of free energy available during each of these chemical reactions was calculated using the following equation to account for non-standard conditions:

$$\Delta G = \Delta G^0 + 2.303\,RT\log Q \quad (5)$$

$$\Delta G = -2.303\,RT\log(K/Q)$$

where ΔG is the Gibbs free energy of reaction (J mol^{-1}); R is the ideal gas constant (8.314 J mol^{-1} K^{-1}); T is the temperature in K; K is the equilibrium constant; and Q is the reaction quotient. K values were calculated using the OBIGT thermodynamic database in CHNOSZ version 2.0.0 (59). The R package CHNOSZ was used to calculate K values for reactions corresponding to experimental conditions (equations 2a, 3, and 4) at pH 3 and 80°C using the subcrt() function. Q values were calculated using measured or calculated concentrations of reactants and products of the reactions. Because these are dilute solutions, activity coefficients were assumed to be 1 for all dissolved compounds (60). [S^{2-}] and [Fe^{2+}] values were estimated based on spectrophotometric measurements, and [Fe^{3+}] values were calculated from the starting [Fe^{3+}] and measured [Fe^{2+}] values. We did not quantify dissolved H_2 concentrations and assumed a constant [H_2] in equilibrium with the H_2/CO_2 headspace (80:20, vol/vol) (ca. 597 µM). The ΔG_{Log} values reported in Table 2 were calculated by taking the average between data points from two time

points that are representative of logarithmic increase in metabolite concentrations (open symbols in Fig. 2).

ACKNOWLEDGMENTS

Financial support was provided by ACS-PRF DNI grant #57209-DNI2 (W.D.L. and Y.W.), the Walter & Constance Burke Fund at Dartmouth College (W.D.L.), the NASA NH Space grant NNX15AH79 (W.D.L. and A.Z.), NSF EAR 1928303 (W.D.L.), the Gordon and Betty Moore Foundation and NSF-1843285 (A.P.), NSF EAR 1820658 (E.B.), the Deutsche Forschungsgemeinschaft grant 441217575 (F.J.E.), and the Dartmouth Society of Fellows (J.H.R.).

The Water-Organic-Rock-Microbe (WORM) Portal was supported by NSF grants EAR-1949030 and EAR-2149016 (G.M.B.).

We thank the other members of the Leavitt, Boyd and Pearson labs for their thoughtful discussion and support.

AUTHOR AFFILIATIONS

[1]Department of Earth Sciences, Dartmouth College, Hanover, New Hampshire, USA
[2]Department of Ecology, Evolution, and Marine Biology, University of California Santa Barbara, Santa Barbara, California, USA
[3]Department of Microbiology and Cell Biology, Montana State University, Bozeman, Montana, USA
[4]School of Earth and Space Exploration, Arizona State University, Tempe, Arizona, USA
[5]Department of Earth and Planetary Sciences, Harvard University, Cambridge, Massachusetts, USA
[6]Leibniz-Laboratory for Radiometric Dating and Isotope Research, Christian-Albrecht University of Kiel, Kiel, Germany
[7]Department of Chemistry, Dartmouth College, Hanover, New Hampshire, USA

PRESENT ADDRESS

Alice Zhou, Department of Earth and Environmental Sciences, University of Michigan, Ann Arbor, Michigan, USA
Maximiliano J. Amenabar, Fundación Científica y Cultural Biociencia, Santiago, Chile
Yuki Weber, Beam Therapeutics, Cambridge, Massachusetts, USA

AUTHOR ORCIDs

Jeemin H. Rhim http://orcid.org/0000-0001-8129-0553
Alice Zhou http://orcid.org/0000-0001-5517-0865
Eric S. Boyd http://orcid.org/0000-0003-4436-5856
William D. Leavitt http://orcid.org/0000-0002-7909-2475

FUNDING

Funder	Grant(s)	Author(s)
American Chemical Society (ACS)	57209-DNI2	Yuki Weber William D. Leavitt
Dartmouth College (Dartmouth)	Walter & Constance Burke Fund	Jeemin H. Rhim William D. Leavitt
National Aeronautics and Space Administration (NASA)	NNX15AH79	Alice Zhou William D. Leavitt
National Science Foundation (NSF)	1928303	William D. Leavitt
Gordon and Betty Moore Foundation (GBMF)		Ann Pearson
National Science Foundation (NSF)	1843285	Ann Pearson
National Science Foundation (NSF)	1820658	Eric S. Boyd

Funder	Grant(s)	Author(s)
Deutsche Forschungsgemeinschaft (DFG)	441217575	Felix J. Elling
National Science Foundation (NSF)	1949030, 2149016	Grayson M. Boyer

ADDITIONAL FILES

The following material is available online.

Supplemental Material

Supplemental material (AEM01369-23-s0001.docx). Additional experimental details, supplementary tables and figures.

REFERENCES

1. Chattopadhyay A, ed. 2017. Membrane organization and Dynamics. Springer International Publishing, Cham.
2. Siliakus MF, van der Oost J, Kengen SWM. 2017. Adaptations of archaeal and bacterial membranes to variations in temperature, pH and pressure. Extremophiles 21:651–670. https://doi.org/10.1007/s00792-017-0939-x
3. Macalady JL, Vestling MM, Baumler D, Boekelheide N, Kaspar CW, Banfield JF. 2004. Tetraether-linked membrane monolayers in *Ferroplasma* spp: a key to survival in acid. Extremophiles 8:411–419. https://doi.org/10.1007/s00792-004-0404-5
4. Oger PM, Cario A. 2013. Adaptation of the membrane in archaea. Biophys Chem 183:42–56. https://doi.org/10.1016/j.bpc.2013.06.020
5. Gliozzi A, Paoli G, De Rosa M, Gambacorta A. 1983. Effect of isoprenoid cyclization on the transition temperature of lipids in thermophilic archaebacteria. Biochimica et Biophysica Acta (BBA)-Biomembr 735:234–242. https://doi.org/10.1016/0005-2736(83)90298-5
6. Jarrell HC, Zukotynski KA, Sprott GD. 1998. Lateral diffusion of the total polar lipids from *Thermoplasma acidophilum* in multilamellar liposomes. Biochim Biophys Acta 1369:259–266. https://doi.org/10.1016/s0005-2736(97)00228-9
7. Gabriel JL, Chong PL. 2000. Molecular modeling of archaebacterial bipolar tetraether lipid membranes. Chem Phys Lipids 105:193–200. https://doi.org/10.1016/s0009-3084(00)00126-2
8. Nicolas JP. 2005. A molecular dynamics study of an archaeal tetraether lipid membrane: comparison with a dipalmitoylphosphatidylcholine lipid bilayer. Lipids 40:1023–1030. https://doi.org/10.1007/s11745-005-1465-2
9. Schouten S, Hopmans EC, Schefuß E, Sinninghe Damsté JS. 2002. Distributional variations in marine crenarchaeotal membrane lipids: a new tool for reconstructing ancient sea water temperatures? Earth Planet Sci Lett 204:265–274. https://doi.org/10.1016/S0012--821X(02)00979-2
10. Schouten S, van der Meer MTJ, Hopmans EC, Rijpstra WIC, Reysenbach A-L, Ward DM, Sinninghe Damsté JS. 2007. Archaeal and bacterial glycerol dialkyl glycerol tetraether lipids in hot springs of Yellowstone National Park. Appl Environ Microbiol 73:6181–6191. https://doi.org/10.1128/AEM.00630-07
11. Powers L, Werne JP, Vanderwoude AJ, Sinninghe Damsté JS, Hopmans EC, Schouten S. 2010. Applicability and calibration of the TEX_{86} paleothermometer in lakes. Org Geochem 41:404–413. https://doi.org/10.1016/j.orggeochem.2009.11.009
12. Pearson EJ, Juggins S, Talbot HM, Weckström J, Rosén P, Ryves DB, Roberts SJ, Schmidt R. 2011. A lacustrine GDGT-temperature calibration from the Scandinavian Arctic to Antarctic: renewed potential for the application of GDGT-paleothermometry in lakes. Geochim Cosmochim Acta 75:6225–6238. https://doi.org/10.1016/j.gca.2011.07.042
13. Pace NR. 1997. A molecular view of microbial diversity and the biosphere. Science 276:734–740. https://doi.org/10.1126/science.276.5313.734
14. Schwartzman DW, Lineweaver CH. 2004. The hyperthermophilic origin of life revisited. Biochem Soc Trans 32:168–171. https://doi.org/10.1042/bst0320168
15. Stetter KO. 2006. Hyperthermophiles in the history of life. Philos Trans R Soc Lond B Biol Sci 361:1837–1842. https://doi.org/10.1098/rstb.2006.1907
16. Shock EL, Holland ME. 2007. Quantitative habitability. Astrobiology 7:839–851. https://doi.org/10.1089/ast.2007.0137
17. De Rosa M, Esposito E, Gambacorta A, Nicolaus B, Bu'Lock JD. 1980. Effects of temperature on ether lipid composition of *Caldariella acidophila*. Phytochemistry 19:827–831. https://doi.org/10.1016/0031-9422(80)85120-X
18. Boyd ES, Pearson A, Pi Y, Li W-J, Zhang YG, He L, Zhang CL, Geesey GG. 2011. Temperature and pH controls on glycerol dibiphytanyl glycerol tetraether lipid composition in the hyperthermophilic crenarchaeon *Acidilobus sulfurireducens*. Extremophiles 15:59–65. https://doi.org/10.1007/s00792-010-0339-y
19. Schouten S, Hopmans EC, Sinninghe Damsté JS. 2013. The organic geochemistry of glycerol dialkyl glycerol tetraether lipids: a review. Org Geochem 54:19–61. https://doi.org/10.1016/j.orggeochem.2012.09.006
20. Jain S, Caforio A, Driessen AJM. 2014. Biosynthesis of archaeal membrane ether lipids. Front Microbiol 5:641. https://doi.org/10.3389/fmicb.2014.00641
21. Jensen SM, Neesgaard VL, Skjoldbjerg SLN, Brandl M, Ejsing CS, Treusch AH. 2015. The effects of temperature and growth phase on the lipidomes of *Sulfolobus islandicus* and *Sulfolobus tokodaii*. Life (Basel) 5:1539–1566. https://doi.org/10.3390/life5031539
22. Elling FJ, Könneke M, Mußmann M, Greve A, Hinrichs K-U. 2015. Influence of temperature, pH, and salinity on membrane lipid composition and TEX_{86} of marine planktonic thaumarchaeal isolates. Geochim Cosmochim Acta 171:238–255. https://doi.org/10.1016/j.gca.2015.09.004
23. Feyhl-Buska J, Chen Y, Jia C, Wang J-X, Zhang CL, Boyd ES. 2016. Influence of growth phase, pH, and temperature on the abundance and composition of tetraether lipids in the thermoacidophile *Picrophilus torridus*. Front Microbiol 7:1323. https://doi.org/10.3389/fmicb.2016.01323
24. Cobban A, Zhang Y, Zhou A, Weber Y, Elling FJ, Pearson A, Leavitt WD. 2020. Multiple environmental parameters impact lipid cyclization in *Sulfolobus acidocaldarius*. Environ Microbiol 22:4046–4056. https://doi.org/10.1111/1462-2920.15194
25. Qin W, Carlson LT, Armbrust EV, Devol AH, Moffett JW, Stahl DA, Ingalls AE. 2015. Confounding effects of oxygen and temperature on the TEX_{86} signature of marine Thaumarchaeota. Proc Natl Acad Sci U S A 112:10979–10984. https://doi.org/10.1073/pnas.1501568112
26. Hurley SJ, Elling FJ, Könneke M, Buchwald C, Wankel SD, Santoro AE, Lipp JS, Hinrichs K-U, Pearson A. 2016. Influence of ammonia oxidation rate on thaumarchaeal lipid composition and the TEX_{86} temperature proxy. Proc Natl Acad Sci U S A 113:7762–7767. https://doi.org/10.1073/pnas.1518534113
27. Zhou A, Weber Y, Chiu BK, Elling FJ, Cobban AB, Pearson A, Leavitt WD. 2020. Energy flux controls tetraether lipid cyclization in *Sulfolobus acidocaldarius*. Environ Microbiol 22:343–353. https://doi.org/10.1111/1462-2920.14851
28. Quehenberger J, Pittenauer E, Allmaier G, Spadiut O. 2020. The influence of the specific growth rate on the lipid composition of *Sulfolobus*

acidocaldarius. Extremophiles 24:413–420. https://doi.org/10.1007/s00792-020-01165-1
29. Elling FJ, Könneke M, Lipp JS, Becker KW, Gagen EJ, Hinrichs K-U. 2014. Effects of growth phase on the membrane lipid composition of the thaumarchaeon *Nitrosopumilus maritimus* and their implications for archaeal lipid distributions in the marine environment. Geochim Cosmochim Acta 141:579–597. https://doi.org/10.1016/j.gca.2014.07.005
30. Evans TW, Könneke M, Lipp JS, Adhikari RR, Taubner H, Elvert M, Hinrichs K-U. 2018. Lipid biosynthesis of *Nitrosopumilus maritimus* dissected by lipid specific radioisotope probing (lipid-RIP) under contrasting ammonium supply. Geochim Cosmochim Acta 242:51–63. https://doi.org/10.1016/j.gca.2018.09.001
31. Amenabar MJ, Shock EL, Roden EE, Peters JW, Boyd ES. 2017. Microbial substrate preference dictated by energy demand rather than supply. Nat Geosci 10:577–581. https://doi.org/10.1038/ngeo2978
32. Amenabar MJ, Colman DR, Poudel S, Roden EE, Boyd ES. 2018. Electron acceptor availability alters carbon and energy metabolism in a thermoacidophile. Environ Microbiol 20:2523–2537. https://doi.org/10.1111/1462-2920.14270
33. Amenabar MJ, Boyd ES. 2018. Mechanisms of mineral substrate acquisition in a thermoacidophile. Appl Environ Microbiol 84:e00334-18. https://doi.org/10.1128/AEM.00334-18
34. Colman DR, Lindsay MR, Harnish A, Bilbrey EM, Amenabar MJ, Selensky MJ, Fecteau KM, Debes RV, Stott MB, Shock EL, Boyd ES. 2021. Seasonal hydrologic and geologic forcing drive hot spring geochemistry and microbial biodiversity. Environ Microbiol 23:4034–4053. https://doi.org/10.1111/1462-2920.15617
35. Urschel MR, Hamilton TL, Roden EE, Boyd ES. 2016. Substrate preference, uptake kinetics and bioenergetics in a facultatively autotrophic, thermoacidophilic crenarchaeote. FEMS Microbiol Ecol 92:fiw069. https://doi.org/10.1093/femsec/fiw069
36. Mathai JC, Missner A, Kügler P, Saparov SM, Zeidel ML, Lee JK, Pohl P. 2009. No facilitator required for membrane transport of hydrogen sulfide. Proc Natl Acad Sci U S A 106:16633–16638. https://doi.org/10.1073/pnas.0902952106
37. Amend JP, Shock EL. 2001. Energetics of overall metabolic reactions of thermophilic and hyperthermophilic archaea and bacteria. FEMS Microbiol Rev 25:175–243. https://doi.org/10.1111/j.1574-6976.2001.tb00576.x
38. Aston JE, Apel WA, Lee BD, Peyton BM. 2009. Toxicity of select organic acids to the slightly thermophilic acidophile *Acidithiobacillus caldus*. Environ Toxicol Chem 28:279–286. https://doi.org/10.1897/08-277.1
39. Capece MC, Clark E, Saleh JK, Halford D, Heinl N, Hoskins S, Rothschild LJ. 2013. Polyextremophiles and the constraints for terrestrial habitability, p 3–59. In Seckbach J, Oren A, Stan-Lotter H (ed), Polyextremophiles. Springer Netherlands, Dordrecht.
40. Pearson A. 2019. Resolving a piece of the archaeal lipid puzzle. Proc Natl Acad Sci U S A 116:22423–22425. https://doi.org/10.1073/pnas.1916583116
41. Hulbert AJ, Else PL. 2005. Membranes and the setting of energy demand. J Exp Biol 208:1593–1599. https://doi.org/10.1242/jeb.01482
42. Ding S, Henkel JV, Hopmans EC, Bale NJ, Koenen M, Villanueva L, Sinninghe Damsté JS. 2022. Changes in the membrane lipid composition of a *Sulfurimonas* species depend on the electron acceptor used for sulfur oxidation. ISME Commun 2:121. https://doi.org/10.1038/s43705-022-00207-3
43. Trincone A, Lanzotti V, Nicolaus B, Zillig W, De Rosa M, Gambacorta A. 1989. Comparative lipid composition of aerobically and anaerobically grown *Desulfwolobus ambivalens*, an autotrophic thermophilic archaeobacterium. Microbiology 135:2751–2757. https://doi.org/10.1099/00221287-135-10-2751
44. Shimada H, Nemoto N, Shida Y, Oshima T, Yamagishi A. 2008. Effects of pH and temperature on the composition of Polar lipids in *Thermoplasma acidophilum* HO-62. J Bacteriol 190:5404–5411. https://doi.org/10.1128/JB.00415-08
45. Laska S, Lottspeich F, Kletzin A. 2003. Membrane-bound hydrogenase and sulfur reductase of the hyperthermophilic and acidophilic archaeon *Acidianus ambivalens*. Microbiology (Reading) 149:2357–2371. https://doi.org/10.1099/mic.0.26455-0
46. Counts JA, Willard DJ, Kelly RM. 2021. Life in hot acid: a genome-based reassessment of the archaeal order *Sulfolobales*. Environ Microbiol 23:3568–3584. https://doi.org/10.1111/1462-2920.15189
47. Urich T, Gomes CM, Kletzin A, Frazão C. 2006. X-ray structure of a self-compartmentalizing sulfur cycle metalloenzyme. Science 311:996–1000. https://doi.org/10.1126/science.1120306
48. Dahl C, Friedrich CG. 2008. Oxidation of sulfur and inorganic sulfur compounds in *Acidianus ambivalens*. In Microbial sulfur metabolism. Springer, Berlin, Heidelberg.
49. Chanda P, Amenabar MJ, Boyd ES, Beard BL, Johnson CM. 2021. Stable Fe isotope fractionation during dissimilatory Fe(III) reduction by a thermoacidophile in acidic hydrothermal environments. Geochim Cosmochim Acta 292:427–451. https://doi.org/10.1016/j.gca.2020.09.025
50. Bennett BD, Gralnick JA. 2019. Mechanisms of toxicity by and resistance to ferrous iron in anaerobic systems. Free Radic Biol Med 140:167–171. https://doi.org/10.1016/j.freeradbiomed.2019.06.027
51. Spietz RL, Payne D, Kulkarni G, Metcalf WW, Roden EE, Boyd ES. 2022. Investigating abiotic and biotic mechanisms of pyrite reduction. Front Microbiol 13:878387. https://doi.org/10.3389/fmicb.2022.878387
52. Boyd ES, Jackson RA, Encarnacion G, Zahn JA, Beard T, Leavitt WD, Pi Y, Zhang CL, Pearson A, Geesey GG. 2007. Isolation, characterization, and ecology of sulfur-respiring crenarchaea inhabiting acid-sulfate-chloride-containing geothermal springs in Yellowstone National Park. Appl Environ Microbiol 73:6669–6677. https://doi.org/10.1128/AEM.01321-07
53. Fogo JK, Popowsky M. 1949. Spectrophotometric determination of hydrogen sulfide. Anal Chem 21:732–734. https://doi.org/10.1021/ac60030a028
54. Viollier E, Inglett PW, Hunter K, Roychoudhury AN, Van Cappellen P. 2000. The ferrozine method revisited: Fe(II)/Fe(III) determination in natural waters. Appl Geochem 15:785–790. https://doi.org/10.1016/S0883-2927(99)00097-9
55. Patwardhan AP, Thompson DH. 1999. Efficient synthesis of 40- and 48-membered tetraether macrocyclic bisphosphocholines. Org Lett 1:241–243. https://doi.org/10.1021/ol990567o
56. Becker KW, Lipp JS, Zhu C, Liu X-L, Hinrichs K-U. 2013. An improved method for the analysis of archaeal and bacterial ether core lipids. Org Geochem 61:34–44. https://doi.org/10.1016/j.orggeochem.2013.05.007
57. Pearson A, Huang Z, Ingalls AE, Romanek CS, Wiegel J, Freeman KH, Smittenberg RH, Zhang CL. 2004. Nonmarine crenarchaeol in Nevada Hot Springs. Appl Environ Microbiol 70:5229–5237. https://doi.org/10.1128/AEM.70.9.5229-5237.2004
58. Zeng Z, Liu X-L, Wei JH, Summons RE, Welander PV. 2018. Calditol-linked membrane lipids are required for acid tolerance in *Sulfolobus acidocaldarius*. Proc Natl Acad Sci U S A 115:12932–12937. https://doi.org/10.1073/pnas.1814048115
59. Dick JM. 2019. CHNOSZ: thermodynamic calculations and diagrams for geochemistry. Front Earth Sci 7:180. https://doi.org/10.3389/feart.2019.00180
60. Spear JR, Walker JJ, McCollom TM, Pace NR. 2005. Hydrogen and bioenergetics in the Yellowstone geothermal ecosystem. Proc Natl Acad Sci U S A 102:2555–2560. https://doi.org/10.1073/pnas.0409574102